DALTON
FULL PAPER

A crystallographic and EPR study of the fluxional Cu(II) ion in $[CuL_2][BF_4]_2$ (L = 2,6-dipyrazol-1-ylpyridine)

Nayan K. Solanki,[a] Michael A. Leech,[b] Eric J. L. McInnes,[c] Frank E. Mabbs,[c] Judith A. K. Howard,[b] Colin A. Kilner,[d] Jeremy M. Rawson[a] and Malcolm A. Halcrow*[d]

[a] *Department of Chemistry, University of Cambridge, Lensfield Road, Cambridge, UK CB2 1EW*
[b] *Department of Chemistry, University of Durham, South Road, Durham, UK DH1 3LE*
[c] *CW EPR Service Centre, Department of Chemistry, University of Manchester, Oxford Road, Manchester, UK M13 9PL*
[d] *School of Chemistry, University of Leeds, Woodhouse Lane, Leeds, UK LS2 9JT. E-mail: M.A.Halcrow@chem.leeds.ac.uk*

Received 9th October 2001, Accepted 21st January 2002
First published as an Advance Article on the web 5th March 2002

This paper reports a crystallographic and EPR study of pseudo-Jahn–Teller fluxionality in $[Cu(L^1)_2][BF_4]_2$ (**1**; L^1 = 2,6-dipyrazol-1-ylpyridine). For $50 \leq T \leq 350$ K, the Cu(II) ion in crystalline **1** is fluxional, with its axis of pseudo-Jahn–Teller elongation being disordered about the two N{pyrazole}–Cu–N{pyrazole} axes. The crystallographic data for **1** at these temperatures are well reproduced by a two-state model that neglects intermolecular interactions, but which yields an unusually small pseudo-Jahn–Teller radius (S_{pJT}) for the compound. This was confirmed by measuring S_{pJT} independently from the mean-square displacement amplitudes (MSDAs) in **1** and $[Zn(L^1)_2][BF_4]_2$ (**2**). At 41 K, **1** undergoes a phase transformation to a new polymorph containing three molecules per asymmetric unit, which have static structures and exhibit more normal S_{pJT} values. Q-band EPR data show that the proportion of static spins in a powdered sample of **1** grows in relatively slowly as the temperature is lowered below 40 K.

Introduction

We have previously demonstrated that $[Cu(L^1)_2][BF_4]_2$ (**1**) adopts a $\{d_{x^2-z^2}\}^1$ electronic ground state in the solid state and in solution (Scheme 1).[1,2] This corresponds structurally to a pseudo-Jahn–Teller elongation of the molecular *x*-axis.[1,3] In solid **1**, this structural elongation is dynamically disordered over the molecular *x*- and *y*-axes;[4–6] such solid-state fluxionality is common in homoleptic Cu(II) complexes of tris-N-donor ligands.[7–9] However, **1** also exhibits a unique, thermally-induced Jahn–Teller switching behaviour involving a crystallographic phase change at 41 K.[3] We now describe a complete variable temperature crystallographic study of **1**, which has allowed us to define the molecular motions occurring in **1** and to understand the origin of this phase change. Variable temperature, multifrequency EPR measurements are also reported. When discussing the low-temperature phase of **1**, the labelling of individual molecules within the asymmetric unit as A, B or C follows that in our original communication.[3]

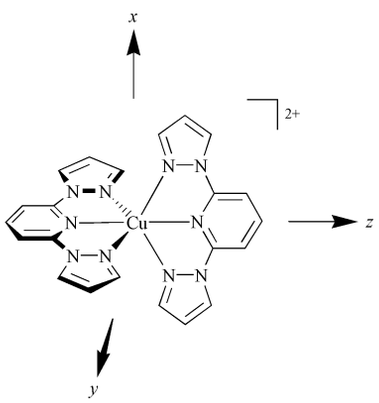

Scheme 1 Molecular axes for $[Cu(L^1)_2]^{2+}$.

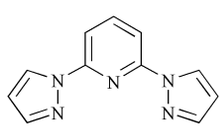

L^1

Results and discussion

Crystallographic investigation of the solid-state fluxionality of 1

A full variable temperature crystallographic study of **1** was undertaken, involving eight datasets collected in the range 350–31 K (see Experimental section). A view of the molecular structure of this complex at 50 K is given in Fig. 1, while the Cu–N distances obtained at each temperature are listed in Table 1. Further details of the bond lengths and angles at each temperature are given in the supplementary information. For the purposes of comparison, structure determinations of the isomorphous Zn(II) complex $[Zn(L^1)_2][BF_4]_2$ (**2**) were also carried out at the same temperatures between 100 and 300 K (Fig. 1). Selected metric parameters for **2** at 100 K are given in Table 2; data for the other temperatures are available in the supplementary information. As expected, the Zn–N distances do not vary significantly over this temperature range, while the N–Zn–N angles at 100 and 300 K are equal to within <2°.

As we have previously communicated,[3] **1** undergoes a crystallographic phase transition at 41 K that does not involve a change in space group ($P2_1$). Rather, in the low-temperature ('LT') phase the crystallographic *b*-axis has trebled in length compared to the high-temperature ('HT') phase. Hence, at 31 K the asymmetric unit contains three crystallographically independent molecules and *Z* has increased from 2 to 6. The BF_4^- anions in **1** and **2** show essentially the same disorder regime at each temperature examined. For T ≥ 200 K, all the F

This journal is © The Royal Society of Chemistry 2002

Table 1 Selected bond lengths (Å) for $[Cu(L^1)_2][BF_4]_2$ (**1**) at different temperatures (d_0 is the average of the six Cu–N distances)

								31[a]		
T/K	350	300	250	200	150	100	50[a]	Molecule A	Molecule B	Molecule C
Cu(1)–N(1)	2.218(5)	2.226(4)	2.223(4)	2.230(4)	2.234(3)	2.2387(14)	2.2527(18)	2.290(2)	2.088(2)	2.306(2)
Cu(1)–N(3)	1.995(3)	2.000(3)	2.005(3)	2.003(3)	2.005(3)	2.0101(11)	2.0175(15)	2.028(2)	1.963(2)	2.026(2)
Cu(1)–N(5)	2.196(5)	2.190(4)	2.189(4)	2.198(4)	2.203(3)	2.2126(14)	2.2259(18)	2.282(2)	2.072(2)	2.266(2)
Cu(1)–N(6)	2.146(5)	2.147(4)	2.142(4)	2.133(4)	2.125(3)	2.1152(14)	2.1080(17)	2.056(2)	2.261(2)	2.058(2)
Cu(1)–N(8)	1.986(3)	1.981(3)	1.981(3)	1.977(3)	1.976(3)	1.9747(10)	1.9763(14)	1.967(2)	2.037(2)	1.958(2)
Cu(1)–N(10)	2.175(4)	2.168(4)	2.156(3)	2.154(4)	2.149(3)	2.1311(13)	2.1210(17)	2.076(2)	2.286(2)	2.077(2)
d_0	2.119(10)	2.119(9)	2.116(9)	2.116(9)	2.115(7)	2.114(3)	2.117(4)	2.117(5)	2.118(5)	2.115(5)

[a] Taken from ref. 3.

Table 2 Selected bond lengths (Å) and angles (°) for $[Zn(L^2)_2](BF_4)_2$ (**2**) at 100 K

Zn(1)–N(1)	2.176(3)
Zn(1)–N(3)	2.097(3)
Zn(1)–N(5)	2.185(3)
Zn(1)–N(6)	2.164(3)
Zn(1)–N(8)	2.107(3)
Zn(1)–N(10)	2.193(3)
N(1)–Zn(1)–N(3)	74.44(12)
N(1)–Zn(1)–N(5)	148.41(12)
N(1)–Zn(1)–N(6)	94.96(12)
N(1)–Zn(1)–N(8)	112.44(13)
N(1)–Zn(1)–N(10)	97.95(12)
N(3)–Zn(1)–N(5)	74.19(13)
N(3)–Zn(1)–N(6)	107.44(11)
N(3)–Zn(1)–N(8)	172.90(13)
N(3)–Zn(1)–N(10)	103.46(10)
N(5)–Zn(1)–N(6)	90.87(12)
N(5)–Zn(1)–N(8)	99.05(13)
N(5)–Zn(1)–N(10)	92.82(11)
N(6)–Zn(1)–N(8)	74.39(11)
N(6)–Zn(1)–N(10)	148.70(12)
N(8)–Zn(1)–N(10)	74.34(11)

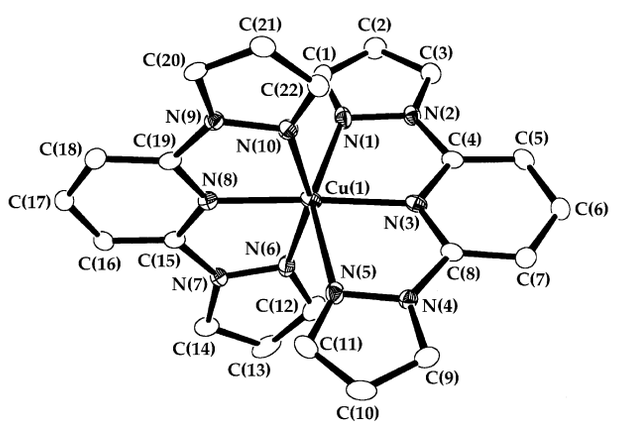

Fig. 1 View of the $[Cu(L^1)_2]^{2+}$ complex dication in the crystal of **1** at 50 K, showing the atom numbering scheme adopted. For clarity, all H atoms have been omitted. Thermal ellipsoids are at the 50% probability level. The $[Zn(L^1)_2]^{2+}$ dication in the crystal of **2** is visually indistinguishable. The same atom numbering scheme for **2** is used, but replacing Cu(1) by Zn(1).

atoms of both anions in their asymmetric units are badly disordered, suggesting that both anions can rotate essentially freely. However, at 150, 100 and (for **1**) 50 K, one of these two anions is now apparently crystallographically ordered, while the other anion has partially ordered so as to be disordered by rotation about one B–F bond. In the LT phase of **1** at 31 K, all six unique BF_4^- anions are crystallographically ordered.

The unit cell parameters of **1** are tabulated in the Experimental section. Between 350–100 K, the unit cell volume ('*V*') of **1** decreases quite uniformly with decreasing temperature, at an average rate of 0.25(3) Å^3 K^{-1}. Interestingly, however, between 100 and 50 K there is a discontinuity, in that *V* is almost equal at these two temperatures. This is reflected in all three of the cell dimensions, which show substantially smaller decreases between 100 and 50 K than expected from the trends at higher temperatures, although the monoclinic angle β does not exhibit this discontinuity. Below the phase transition, at 31 K, the cell volume occupied by two formula units (*i.e.* *V*/3) has again decreased, at a similar rate to that exhibited above 100 K.

The coordination sphere of the Cu ion in **1** is rhombic at all the temperatures examined (Table 1). As the temperature is decreased from 350–50 K there is a smooth increase in the apparent Cu–N distances along the molecular *x*-axis [Cu(1)–N(1) and Cu(1)–N(5)], and a corresponding decrease in the *y*-axis Cu–N bond lengths [Cu(1)–N(6) and Cu(1)–N(10)]. This is consistent with an increasing relative population of one well of the Mexican Hat potential surface that describes the pseudo-Jahn–Teller distortion of **1**,[5] as the temperature is lowered. Similar trends have been observed previously in variable temperature X-ray studies of the fluxional complexes $[Cu(NO_2)(bipy)_2]NO_3$,[6] $[Cu(NO_2)(bipyam)_2]ClO_4$ (bipyam = bis{pyrid-2-yl}amine),[10] $[H_3NC_6H_4Cl\text{-}3]_2[CuCl_6]$,[11] $[Cu(OH_2)_2(O_2CCH_2OMe)_2]$,[12] $(ND_4)_2[Cu(D_2O)_6][SO_4]_2$[13] and $[Cu(C_6H_9\{OH\}_3\text{-}1,3,5)_2][Ots]_2$.[14] However, at 50 K, the apparent coordination sphere at Cu still exhibits a relatively small rhombic elongation compared to related literature compounds such as $[Cu(terpy)_2][NO_3]_2$[15] (see below). Between 50 and 31 K, which span the phase transition undergone by **1** at 41 K, the Cu–N bond lengths change substantially, leading to a coordination geometry that is now more typical of a pseudo-Jahn–Teller-elongated Cu(II) species (Table 1). The average Cu–N distance in the dication is identical within experimental error at all the temperatures examined (Table 1).

The vibrational amplitudes of the ligand donor atoms along the six Cu–N bonds of the complex can be represented by the quantity $\langle d^2 \rangle$.[5,16] This corresponds to the difference in the mean-square displacement parameters (MSDAs) of a given N atom and the Cu atom along their common vector (eqn. 1 and 2).

$$\text{MSDA} = \frac{\sum_{i=1}^{3}\sum_{j=1}^{3} U_{ij} n_i n_j}{|n|^2} \quad (1)$$

$$\langle d^2 \rangle = \text{MSDA (N)} - \text{MSDA (Cu)} \quad (2)$$

where U_{ij} is an element of the 3 × 3 matrix of thermal parameters and n_i and n_j are elements of the vector describing the bond. It has been suggested that disordered Cu–N bonds *generally* yield $\langle d^2 \rangle \geq 0.010$.[17] At 50 ≤T ≤ 300 K, $\langle d^2 \rangle$ for Cu(1)–N(1) and Cu(1)–N(6) is generally greater than this threshold value, and is substantially larger than for the other Cu–N bonds in **1** (Table 3). Since the variation in Cu–N bond lengths with temperature shows that *all* the Cu–N bonds in **1** are in fact fluxional, the lower values of $\langle d^2 \rangle$ for Cu(1)–N(5) and

Table 3 Calculated $\langle d^2 \rangle$ (10^4 Å^2), $\langle d^2 \rangle_{corr}$ (10^4 Å^2) and S_{pJT} values for **1** and **2**. A negative value of $\langle d^2 \rangle$ arises when MSDA (N) < MSDA (M). Estimated errors on $\langle d^2 \rangle$ are ±20 10^4 Å^2, and are ±30 10^4 Å^2 on $\langle d^2 \rangle_{corr}$. The S_{pJT} values for 300 ≤ T ≤ 100 K were calculated from eqn. 6, while those at 31 K were calculated using eqn. 7

T/K	M(1)–N(1)	M(1)–N(3)	M(1)–N(5)	M(1)–N(6)	M(1)–N(8)	M(1)–N(10)	S_{pJT}
Complex **1** (M = Cu) $\langle d^2 \rangle$							
350	137	−37	58	177	−6	28	
300	141	−15	93	153	−12	68	0.17(5)
250	105	−29	82	140	−31	88	0.14(5)
200	86	−40	76	139	−40	51	0.13(5)
150	90	−13	74	123	−51	81	0.10(5) [0.12(5)[a]]
100	95	−13	54	118	−38	52	0.11(5)
50	111	5	63	116	−24	59	
31 (Molecule A)	14	6	28	29	34	40	0.305(6)
31 (Molecule B)	42	15	89	31	12	49	0.287(6)
31 (Molecule C)	48	18	44	41	22	43	0.311(6)
Complex **1** (M = Cu) $\langle d^2 \rangle_{corr}$							
300	81	−46	83	178	−78	59	
250	57	−45	60	114	−58	74	
200	59	−62	78	126	−73	43	
150[b]	55 [55]	−55 [−14]	61 [33]	70 [81]	−73 [−88]	44 [67]	
100	56	−23	26	61	−39	34	
Complex **2** (M = Zn) $\langle d^2 \rangle$							
300	60	31	7	−25	66	9	
250	48	16	22	26	27	14	
200	27	22	−2	13	33	8	
150[b]	35 [35]	42 [1]	13 [41]	53 [42]	22 [37]	37 [14]	
100	39	10	28	57	−1	18	

[a] This value of S_{pJT} was calculated using the alternative dataset of **2** collected at 150 K. [b] Values in square brackets were obtained from a second dataset aquired from a different crystal of **2**.

Cu(1)–N(10), and the negative values shown by Cu(1)–N(3) and Cu(1)–N(8), suggest that the Jahn–Teller-induced vibration of the L^1 ligands in **1** may be coupled to motion of the Cu ion. We note that our determinations of **1** at 50 and 100 K used a different crystal and diffractometer from those at 150–350 K, but show the same pattern of $\langle d^2 \rangle$ values. Hence, the observed $\langle d^2 \rangle$ values should not be strongly affected by systematic influences of the crystal or data collection on the atomic displacement ellipsoids. At 31 K, $\langle d^2 \rangle$ is positive and <0.010 for all 18 independent Cu–N bonds, showing that all three independent Cu ions have static molecular structures in the LT phase.

The same trends as described above are observed in the corrected $\langle d^2 \rangle$ values for **1** between 100 and 300 K (eqn. 3).

$$\langle d^2 \rangle_{corr} = \langle d^2 \rangle_{obs} - \langle d^2 \rangle_{res} \quad (3)$$

where the observed and residual $\langle d^2 \rangle$ values represent $\langle d^2 \rangle$ for the Cu and Zn complexes, respectively, at a given temperature (Table 3). This correction eliminates the (minor) contributions from other Cu–N vibrational modes and, to some extent, from other systematic contributions to the crystallographic thermal ellipsoids. Unfortunately, however, the relatively small values of $\langle d^2 \rangle$ exhibited by **1** and **2**, coupled with the larger errors introduced into $\langle d^2 \rangle_{corr}$, make the latter a less useful comparative tool than the uncorrected $\langle d^2 \rangle$ values for this system.

The Cu–N bond lengths for **1** were analysed according to the model of Silver and Getz,[18] as modified by Simmons *et al.*[6] This model describes a molecule equilibrating between its two lowest energy vibronic minima, separated by energy ΔE. All higher energy vibronic levels, and intermolecular interactions that might lead to cooperative fluxionality within the solid, are ignored. According to this model, the equilibrium constant can be written as eqn. 4

$$K = \frac{S_{pjt} + S'}{S_{pjt} - S'} \quad (4)$$

where S' (the distortion coordinate) is defined by eqn. 5 (see Fig. 1 for the atom numbering scheme)

$$S'^2 = \frac{1}{2}\left\{ \begin{array}{r} [(Cu(1)–N(3))–(Cu(1)–N(8))]^2 + \\ [(Cu(1)–N(5))–(Cu(1)–N(6))]^2 + \\ [(Cu(1)–N(1))–(Cu(1)–N(10))]^2 \end{array} \right\} \quad (5)$$

and S_{pJT} (also known as the pseudo-Jahn–Teller radius, R_{PJT}[5,16]), is the value of S' at the static limit. The constant S_{pJT} can be derived by performing trial plots of ln$K$ *vs.* $1/T$, using different values of S_{pJT} until a linear graph is obtained. Using this method, for 50 ≤ T ≤ 350 K, a value of S_{pJT} = 0.130 gave a good straight-line graph with a correlation coefficient of 0.995, that passes very close to the origin, as required by the model [intercept −0.02; Fig. 2(a)]. The slope of this line affords the energy gap between the two vibronic minima, ΔE = 173 cm^{-1}, which compares well with similar determinations from other fluxional Jahn–Teller complexes.[6,10,19]

Alternatively, S_{pJT} can be measured directly by comparison of the compound under study with the crystal structure of its Zn(II)-containing congener, using eqn. 6.

$$S_{pjt}^{\ 2} = \sum_{i=1}^{6} \langle d_j^2 \rangle_{corr} \quad (6)$$

where $\langle d_i^2 \rangle_{obs}$ and $\langle d_i^2 \rangle_{res}$ represent $\langle d^2 \rangle$ for the ith M–N bond in the Cu and Zn complexes **1** and **2**, respectively.[16] The values of S_{pJT} calculated from this equation between 100 and 300 K are identical to within experimental error (Table 3). As a control, S_{pJT} was also calculated at 150 K using a dataset collected from a different crystal of **2**; the two values of S_{pJT} calculated at this temperature are also identical (Table 3). At all these temperatures, S_{pJT} measured using eqn. 6 corresponds well to the value of 0.130 derived by the interpolation procedure above.

There are two anomalies about this value of S_{pJT}. First, it cannot describe the LT phase of **1**, since infinite values of ln$K$ at

Table 4 Selected Q-band EPR data for **1**. Hyperfine couplings are to ^{63,65}Cu and are in G. Unless otherwise stated, estimated errors in g are ±0.002, and in A are ±3 G. The solution spectrum was run in 10 : 1 MeCN : toluene

		Major species				Minor species			
T/K	Phase	g_1	g_2	g_3	A_1	g_1	g_2	g_3	A_1
290	Powder	2.195	2.195	2.043	—				
120	Powder	2.228	2.160	2.040	—				
60	Powder	2.230	2.155	2.041	—				
40	Powder	2.228	2.148	2.042	—				
5	Powder	2.210	2.133	2.042	—	2.32[a]	2.093	2.042	200[b]
120	MeCN	2.281	2.099	2.051	137	—	—	—	—

[a] Estimated error on this g-value is ±0.04. [b] Estimated error on this coupling constant is ±50 G.

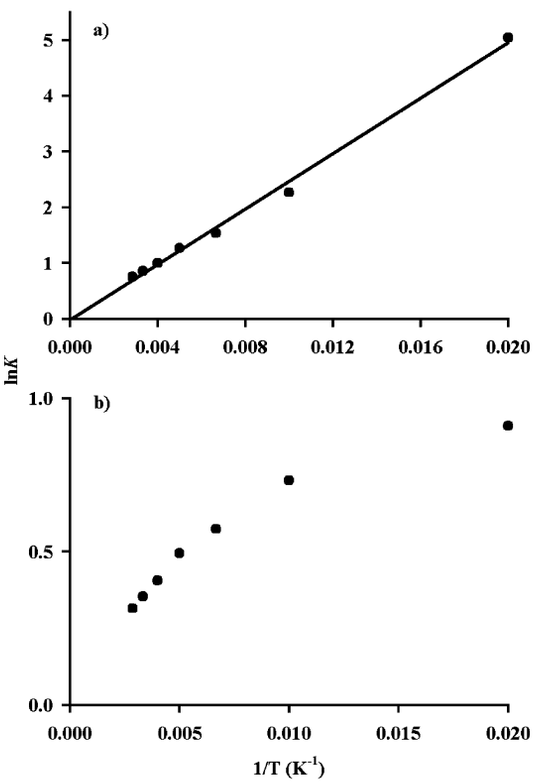

Fig. 2 Plot of ln$K$ *vs.* 1/T for the high-temperature phase of **1** according to the Silver and Getz model: (a) for S_{pJT} = 0.130, showing the line of best fit; (b) for S_{pJT} = 0.301.

31 K are obtained from eqn. 2 for S_{pJT} = 0.130. Second, a value of S_{pJT} = 0.130 is unusually low compared to other Cu(II) complexes.[16] Both of these facts imply that the pseudo-Jahn–Teller radius S_{pJT} = 0.130 derived from the HT phase of **1** does not in fact represent its ground state molecular structure. This was confirmed by derivation of S_{pJT} for **1** at 31 K using eqn. 7, which is valid for non-fluxional pseudo-Jahn–Teller-distorted structures.[5]

$$S_{pjt}{}^2 = \sum_{i=1}^{6}(d_0 - d_i^2) \qquad (7)$$

where d_0 is the average Cu–N distance (Table 1) and d_i is the length of the ith Cu–N bond. By this method, values of S_{pJT} in the range 0.287(6)–0.311(6) were calculated for the three crystallographically independent molecules in the 31 K structure of **1** (Table 3); these are now very comparable with values calculated from other Jahn–Teller-distorted Cu(II) compounds containing hexa-nitrogen donor sets, which are usually close to 0.32.[16] In particular, $[Cu(terpy)_2][NO_3]_2$, whose coordination sphere should have a similar plasticity to that of **1**, exhibits S_{pJT} = 0.308(14).[15] For comparable static and fluxional molecular structures of the same compound, eqn. 6 and 7 should give identical values of S_{pJT};[16] clearly, this is not true for **1**. Attempts to fit the X-ray data for the HT phase of **1** using S_{pJT} = 0.301 (the average value of S' at 31 K for the three molecules in the asymmetric unit) gave a highly curved graph [Fig. 2(b)]. Hence, it is clear that the phase change exhibited by **1** involves a change in its fluxionality.

EPR study of the solid-state fluxionality in 1

The fluxionality in solid **1** was also studied by Q-band EPR spectroscopy, performed on powdered crystals of the complex (Fig. 3). At 290 K the spectrum is axial at this frequency, with an 'inverse' g-pattern of $g_\perp > g_\parallel > g_e$ that is characteristic of an exchange-averaged crystal or molecular spectrum, associated with a fluxional pseudo-Jahn–Teller-elongated spin.[1,4–6,20] At 120 K the spectrum has become rhombic, while between 120 and 40 K the g-values show only small differences, associated mostly with a small decrease in g_2 (Table 4). Below 40 K, the spectrum is more complex (Fig. 3) and can only be simulated by assuming the presence of two spin systems. The major spin system has g-values that are similar to those above 40 K, and no resolvable hyperfine coupling. However, the minor spin exhibits detectable ^{63,65}Cu hyperfine coupling on g_1, and shows g-values that resemble those of **1** in solution and are more typical of a $\{d_{y^2-z^2}\}^1$ Cu(II) ion (Table 4).[21] This is consistent with the powder sample containing a mixture of fluxional (major) and static (minor) Cu(II) centres at these temperatures.

Accurate simulations of the low-temperature powder spectra could not be obtained (Table 4), because the $A_1\{^{63,65}Cu\}$ lines

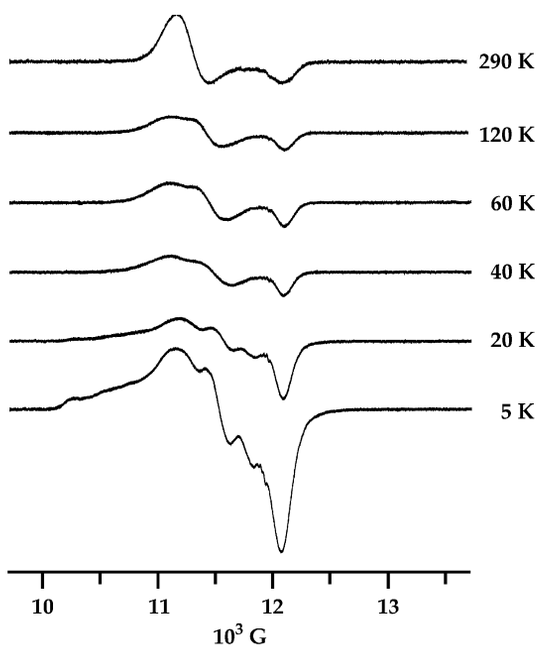

Fig. 3 Variable temperature Q-band EPR study of powdered **1**.

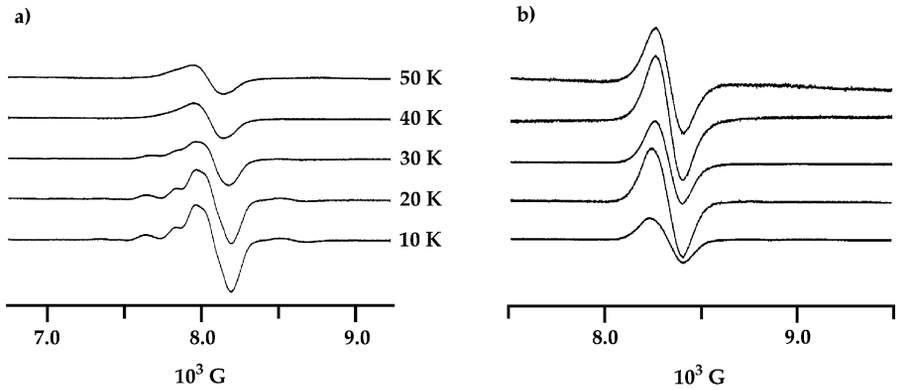

Fig. 4 K-band single crystal EPR spectra of **1** aligned parallel to the crystallographic (a) *b*- and (b) *c*-axes.

from the minor spin system are extremely broad, leading to large errors on g_1 and A_1 for this spin. However, it is clear that the proportion of static Cu(II) spins increases at the expense of fluxional Cu(II) ions as the temperature is lowered between 40 and 5 K, reaching a relative population of *ca.* 1 : 2 at 5 K. It is also apparent that the *g* and *A* values of both spin systems do not change significantly between these temperatures (Fig. 3). These data imply that, below 40 K, the powder sample contains a mixture of static and fluxional $\{d_{y^2-z^2}\}^1$ Cu(II) centres, and that the population of the former increases at the expense of the latter as the temperature is lowered.

Since the LT phase of crystalline **1** contains only static Cu(II) centres, it is likely that the onset of mixed time-averaged and static spectra for powdered **1** below 40 K is connected with its 41 K phase transition. The slow increase in the relative population of static spins with decreasing temperature suggests that, in the powder sample, the phase transition is much less abrupt than in the single crystal. Similar observations have been made previously regarding the related phenomenon of thermal spin-crossover transitions in Fe(II) complexes, where the width of the transition can be very dependent on the particle size, and method of preparation, of the solid sample.[22]

In an attempt to further resolve the low-temperature *g*-values of **1**, a variable temperature powder EPR study of **1** at 90 GHz was also attempted. Above 40 K, the 90 GHz spectra closely mirror those obtained at Q-band (at 300 K, $g_\perp = 2.190$, $g_\parallel = 2.035$; at 60 K, $g_1 = 2.220$, $g_2 = 2.145$, $g_3 = 2.035$). Below 40 K, in agreement with the Q-band data, the 90 GHz spectra become rather more complex. These latter spectra are more complicated than those at Q-band, however, and thus far we have been unable to simulate these low-temperature spectra accurately.

A preliminary EPR study was carried out on neat single crystals of **1** at K-band. Spectra along the three principle crystallographic axes were recorded, at varying temperatures between 5–290 K. The spectra parallel to the crystallographic *c*-direction at all temperatures present a single line at $g = 2.055 \pm 0.003$ [Fig. 4(b)]. This should be close to the true value of g_z, since the molecular *z*-axes (Scheme 1) of all molecules in the unit cells of both modifications of **1** lie almost parallel to the crystallographic *c*-vector. The spectra parallel to *a* and *b* are apparently isotropic above 40 K, with temperature-dependent $\langle g \rangle$ values [Fig. 4(a)]. However, below 40 K, additional features implying the presence of more than one spin (including ^{63,65}Cu hyperfine interactions) grow into these spectra; these changes are reversible upon raising the temperature. Since the molecular *x*- and *y*-axes for the molecules in the unit cell in both phases of **1** do not lie parallel to the crystallographic *a*- or *b*-directions, a detailed interpretation of the data obtained along *a* or *b* is not possible at present. However, because these spectra will be composed purely of admixtures of g_x and g_y, they provide additional evidence that the temperature changes in the EPR spectrum of solid **1** are associated with the pseudo-Jahn–Teller fluxionality of this complex. A complete, multi-orientation variable temperature single crystal EPR study of **1** is in progress, and will be reported separately.

Concluding remarks

Through the analyses described above, it is clear that the HT and LT phases of **1** exhibit different pseudo-Jahn–Teller regimes. We have shown that the HT phase is fluxional between 50–350 K, while all three of the independent molecules in the LT phase have static structures that are very similar to the structures of closely related, non-fluxional Cu(II) complexes. The HT fluxionality can be fitted well to the Silver and Getz two-state equilibrium model, using a static distortion coordinate S_{pJT} that was measured independently, but which cannot be applied to the structure of the LT phase. The Silver and Getz approach assumes that the molecules in **1** vibrate independently of each other,[6,18] which is consistent with the observation that fluxional **1** and static **2** exhibit the same anion disorder at every temperature at which the compounds were analysed. This suggests that the cation fluxionality and anion motion in **1** are not coupled, except at temperatures approaching the phase transition.[3] It should be noted that, although the model describes motion of the ligand N-donor atoms only (omitting the rest of the ligand framework), this gross approximation should not cause significant errors in the calculated parameters.[16]

It is noteworthy that the value of S_{pJT} for the 50–350 K data (0.130) is very close to S' at 50 K (0.128), suggesting that at 50 K the system is very near the static limit in this phase. The small value of S_{pJT} from this analysis would mean that the Q(θ) and Q(ε) vibrations of the CuN_6 octahedron, which define the Mexican Hat potential surface for the pseudo-Jahn–Teller distortion of **1**,[5] have unusually small amplitudes in the HT phase. That is, the true molecular structure of **1** in its HT phase is only slightly different from that of a non-Jahn–Teller-active $[M(L^1)_2]^{2+}$ species.[23–25] This quenching of the Jahn–Teller effect would be imposed by the surrounding HT lattice, since the LT phase of **1** exhibits a normal pseudo-Jahn–Teller elongation. While the data we have presented are self-consistent and support this interpretation, a lattice-quenched Jahn–Teller distortion of this type would be highly unusual. However, it is also possible that the agreement of our data with the Silver and Getz model is coincidental, and that the cation fluxionality in **1** is in fact cooperative. It is suggestive in this regard that $[Fe(L^1)_2][BF_4]_2$, which is isomorphous with **1**, undergoes an abrupt spin-state transition that implies a degree of cooperativity between Fe centres in the solid.[24,25] We are attempting to further define the lattice strain energies in **1** using single crystal near-IR and EPR,[13,15] and EXAFS,[26] experiments; the results of these studies will be reported separately.

Experimental

Unless stated otherwise, all manipulations were performed in air. Complex **1** [1] and L^1 [27] were prepared by the literature

Table 5 Experimental details for the single crystal structure determinations of $[Cu(L^1)_2](BF_4)_2$ (**1**, $C_{22}H_{18}B_2CuF_8N_{10}$, M_r 659.62) at different temperatures

T/K	350(2)	300(2)	250(2)	200(2)	150(2)	100(2)	50(2)[a]	31(2)[a]
Crystal class	Monoclinic	Monoclinic	Monoclinic	Monoclinic	Monoclinic	Monoclinic	Monoclinic	Monoclinic
Space group	$P2_1$	$P2_1$	$P2_1$	$P2_1$	$P2_1$	$P2_1$	$P2_1$	$P2_1$
a/Å	8.5234(2)	8.4981(2)	8.4734(2)	8.4547(2)	8.4377(2)	8.4158(4)	8.4141(9)	8.4047(6)
b/Å	8.5849(2)	8.5663(2)	8.5454(2)	8.5258(2)	8.5069(2)	8.4834(4)	8.4747(9)	25.3897(18)
c/Å	19.0161(4)	18.9448(5)	18.8745(6)	18.8122(7)	18.7544(7)	18.6853(8)	18.6833(19)	18.6676(13)
β/°	95.6764(11)	96.1310(11)	96.4846(9)	96.7596(11)	96.9618(11)	97.147(1)	97.371(2)	97.205(1)
V/Å^3	1384.63(5)	1371.24(6)	1357.93(6)	1346.61(7)	1336.24(7)	1323.66(11)	1321.2(2)	3952.1(5)
Z	2	2	2	2	2	2	2	6
μ(Mo-Kα)/mm^{-1}	0.876	0.885	0.893	0.901	0.908	0.916	0.918	0.921
Measured reflections	17357	14125	12673	12512	12593	16352	12227	23287
Independent reflections	5410	5522	5840	5799	5757	6955	5261	9396
R_{int}	0.049	0.038	0.035	0.045	0.047	0.017	0.016	0.027
$R(F)$[b]	0.053	0.045	0.046	0.48	0.043	0.022	0.022	0.027
w$R(F^2)$[c]	0.145	0.124	0.118	0.115	0.103	0.058	0.066	0.074
Flack parameter	−0.002(18)	−0.018(15)	0.011(14)	0.007(15)	−0.018(12)	0.553(5)	0.553(7)	0.549(10)

[a] Taken from ref. 3. [b] $R = \Sigma[|F_o| - |F_c|]/\Sigma|F_o|$. [c] $wR = [\Sigma w(F_o^2 - F_c^2)/\Sigma wF_o^4]^{1/2}$.

Table 6 Experimental details for the single crystal structure determinations of $[Zn(L^1)_2](BF_4)_2$ (**2**, $C_{22}H_{18}B_2F_8N_{10}Zn$, M_r = 661.45) at different temperatures

T/K	300(2)	250(2)	200(2)	150(2)	150(2)[a]	100(2)
Crystal class	Monoclinic	Monoclinic	Monoclinic	Monoclinic	Monoclinic	Monoclinic
Space group	$P2_1$	$P2_1$	$P2_1$	$P2_1$	$P2_1$	$P2_1$
a/Å	8.5022(2)	8.4863(2)	8.4726(2)	8.4605(2)	8.4635(2)	8.4533(2)
b/Å	8.5044(3)	8.5234(2)	8.5038(2)	8.4808(3)	8.4801(2)	8.4620(3)
c/Å	19.0408(8)	18.9687(6)	18.8988(5)	18.8377(6)	18.8401(6)	18.7922(6)
β/°	95.9483(13)	96.2969(11)	96.5478(10)	96.744(2)	96.8011(12)	96.9787(12)
V/Å^3	1369.35(7)	1363.77(6)	1352.76(6)	1342.29(7)	1342.66(6)	1334.28(7)
Z	2	2	2	2	2	2
μ(Mo-Kα)/mm^{-1}	0.985	0.989	0.997	1.005	1.005	1.011
Measured reflections	10963	11123	11227	11393	10224	11234
Independent reflections	5505	5405	5441	5526	5615	5467
R_{int}	0.040	0.046	0.037	0.048	0.038	0.052
$R(F)$[b]	0.051	0.046	0.038	0.046	0.040	0.044
$wR(F^2)$[c]	0.137	0.117	0.099	0.105	0.092	0.100
Flack parameter	−0.015(17)	0.015(14)	0.002(12)	0.009(13)	0.004(11)	−0.006(12)

[a] Data collected using a different crystal. See Experimental section. [b] $R = \Sigma[|F_o| - |F_c|]/\Sigma|F_o|$. [c] $wR = [\Sigma w(F_o^2 - F_c^2)/\Sigma wF_o^4]^{1/2}$.

procedures. $Zn[BF_4]_2 \cdot 6H_2O$ (Avocado) and all solvents (analytical grade) were used as supplied.

Synthesis of bis[2,6-di(pyrazol-1-yl)pyridine]zinc(II) ditetrafluoroborate (2)

A solution of L^1 (0.80 g, 2.4×10^{-3} mol) and $Zn[BF_4]_2 \cdot 6H_2O$ (0.44 g, 1.2×10^{-3} mol) in MeCN (30 cm^3) was stirred for 10 min at room temperature. The colourless solution was filtered and concentrated to *ca.* 5 cm^3. Vapor diffusion of Et_2O into this solution gave colourless microcrystals. Yield 0.97 g, 86%. Found: C, 39.8; H, 2.7; N, 20.9; calcd. for $C_{22}H_{18}B_2F_8N_{10}Zn$: C, 40.0; H, 2.7; N, 21.2%. FAB mass spectrum: *m*/*z* 487 $[^{64}Zn(L^1)_2 + H]^+$, 295 $[^{64}ZnF(L^1)]^+$, 276 $[^{64}Zn(L^1)]^+$.

Single crystal X-ray structure determinations

Single crystals of **1** and **2** were grown by vapour diffusion of Et_2O into MeCN solutions of the complexes. Experimental details from the structure determinations are given in Tables 5 and 6. Data for **1** at 31, 50 and 100 K were obtained using a Siemens SMART diffractometer fitted with an Oxford Cryosystems HELIX helium cooling device. All other data were collected using an Enraf Nonius KappaCCD diffractometer fitted with an Oxford Cryosystems nitrogen cooling device. Crystals were mounted on a glass ($T \geq 100$ K) or nylon ($T \leq 50$ K) fibre using a drop of perfluoropolyether oil. Experimental details from the structure determinations are given in Tables 5 and 6. All structures were solved by direct methods (SHELXS 86[28]) and refined by full matrix least-squares on F^2 (SHELXL 97[29]). For all the structure determinations, all H atoms were placed in calculated positions. Mean-square diplacement parameters were calculated using the program THMA11,[30] incorporated into the WinGX suite of crystallographic software.[31]

CCDC reference numbers 137102, 137103 and 172160–172171.

See http://www.rsc.org/suppdata/dt/b1/b109201b/ for crystallographic data in CIF or other electronic format.

$[Cu(L^1)_2][BF_4]_2$ (1). Eight datasets were collected for this compound between 31 and 350 K. One crystal was used to collect data between 150 and 350 K, while a second crystal was employed for data collection at 31–100 K; the latter crystal was a racemic twin. The structure determination at 31 K contained no disorder. For T = 50 and 100 K, one BF_4^- anion was disordered by rotation about one B–F bond, over two distinct orientations that refined to 0.69 : 0.31 (50 K) and 0.55 : 0.45 (100 K). No restraints were applied at these three temperatures and all non-H atoms were refined anisotropically. At 150 K, this anion was disordered over three orientations by rotation about the same B–F bond, with estimated occupancy ratios of 0.50 : 0.25 : 0.25. At 200 K and above, both BF_4^- anions were badly disordered. All the F atoms of one anion were modeled over three orientations in a 0.40 : 0.40 : 0.20 occupancy ratio, while for the other anion, four distinct F-atom orientations were modeled with occupancies of 0.40 : 0.20 : 0.20 : 0.20; the first three of these were related by rotation about one B–F bond. All disordered B–F bonds were restrained to a given value which ranged from 1.38(2)–1.40(2) Å at different temperatures, while all non-bonded F ··· F distances within a given disorder orientation were restrained to 2.25(2)–2.29(2) Å. At 150–350 K, all non-H atoms with occupancies ≥0.5 were refined anisotropically.

$[Zn(L^1)_2][BF_4]_2$ (2). Datasets were collected for this complex between 100 and 300 K at 50 K intervals, using the same crystal at all temperatures. For $T = 100$ and 150 K, one BF_4^- anion was disordered by rotation about one B–F bond, over three distinct orientations with an occupancy ratio of 0.50 : 0.25 : 0.25. For $T \leq 200$ K, both anions were badly disordered. This was modeled employing the same regime of partial F-atom occupancies and restraints as used for **1** at the same temperatures. For all five structures, all non-H atoms with occupancies ≥0.5 were refined anisotropically.

Other measurements

Positive ion fast atom bombardment mass spectra were performed on a Kratos MS890 spectrometer, employing a 3-NOBA matrix. CHN microanalyses were performed by the University of Cambridge Department of Chemistry microanalytical service. EPR spectra were obtained using a Bruker ESP300E spectrometer; Q-band spectra employed an ER5106QT resonator and ER4118VT cryostat, while for K-band spectra an ER6706KT resonator and ER4118CF cryostat were used. Spectral simulations were performed using in-house software which has been described elsewhere.[32]

Acknowledgements

The authors thank Dr Michael Hitchman (University of Tasmania) and Dr Gavin Reid (University of Leeds) for useful discussions. Financial support is acknowledged from the Royal Society (London) for a research fellowship to M. A. H., the EPSRC (N. K. S., M. A. L.), ICI R&T Division (N. K. S.), the University of Cambridge and the University of Leeds.

References

1 N. K. Solanki, E. J. L. McInnes, F. E. Mabbs, S. Radojevic, M. McPartlin, N. Feeder, J. E. Davies and M. A. Halcrow, *Angew. Chem., Int. Ed.*, 1998, **37**, 2221.
2 A. J. Bridgeman, M. A. Halcrow, M. Jones, E. Krausz and N. K. Solanki, *Chem. Phys. Lett.*, 1999, **314**, 176.
3 M. A. Leech, N. K. Solanki, M. A. Halcrow, J. A. K. Howard and S. Dahaoui, *Chem. Commun.*, 1999, 2245.
4 M. A. Hitchman, *Comments Inorg. Chem.*, 1994, **15**, 197.
5 L. R. Falvello, *J. Chem. Soc., Dalton Trans.*, 1997, 4463.
6 C. J. Simmons, B. J. Hathaway, K. Amornjarusiri, B. D. Santarsiero and A. Clearfield, *J. Am. Chem. Soc.*, 1987, **109**, 1947.
7 J.-V. Folgado, W. Henke, R. Allmann, H. Stratemeier, D. Beltrán-Porter, T. Rojo and D. Reinen, *Inorg. Chem.*, 1990, **29**, 2035.
8 M. Duggan, B. J. Hathaway and J. Mullane, *J. Chem. Soc., Dalton Trans.*, 1980, 690.
9 J. M. Holland, X. Liu, J. P. Zhao, F. E. Mabbs, C. A. Kilner, M. Thornton-Pett and M. A. Halcrow, *J. Chem. Soc., Dalton Trans.*, 2000, 3316.
10 C. J. Simmons, *New J. Chem.*, 1993, **17**, 77.
11 M. Wei and R. D. Willett, *Inorg. Chem.*, 1995, **34**, 3780.
12 K. J. Prout, A. Edwards, V. Mtetwa, J. Murray, J. F. Saunders and F. J. C. Rossotti, *Inorg. Chem.*, 1997, **36**, 2820.
13 M. A. Hitchman, W. Maaskant, J. van der Plas, C. J. Simmons and H. Stratemeier, *J. Am. Chem. Soc.*, 1999, **121**, 1488.
14 J. Bebendorf, H.-B. Bürgi, E. Gamp, M. A. Hitchman, A. Murphy, D. Reinen, M. J. Riley and H. Stratemeier, *Inorg. Chem.*, 1996, **35**, 7419.
15 R. Allmann, W. Henke and D. Reinen, *Inorg. Chem.*, 1978, **17**, 378.
16 J. H. Ammeter, H. B. Bürgi, E. Gamp, V. Meyer-Sandrin and W. P. Jensen, *Inorg. Chem.*, 1979, **18**, 733.
17 B. J. Hathaway, *Struct. Bonding (Berlin)*, 1984, **57**, 55.
18 B. L. Silver and D. Getz, *J. Chem. Phys.*, 1974, **61**, 638.
19 N. W. Alcock, M. Duggan, A. Murray, S. Tyagi, B. J. Hathaway and A. Hewat, *J. Chem. Soc., Dalton Trans.*, 1984, 7.
20 D. Reinen and M. A. Hitchman, *Z. Phys. Chem.*, 1997, **200**, 11.
21 B. A. Goodman and J. B. Raynor, *Adv. Inorg. Chem.*, 1970, **13**, 135.
22 E. W. Müller, H. Spiering and P. Gütlich, *Chem. Phys. Lett.*, 1982, **93**, 567.
23 J. M. Holland, C. A. Kilner, M. Thornton-Pett and M. A. Halcrow, *Polyhedron*, 2001, **20**, 2829.
24 J. M. Holland, J. A. McAllister, Z. Lu, C. A. Kilner, M. Thornton-Pett and M. A. Halcrow, *Chem. Commun.*, 2001, 577.
25 J. M. Holland, J. A. McAllister, C. A. Kilner, M. Thornton-Pett, A. J. Bridgeman and M. A. Halcrow, *J. Chem. Soc., Dalton Trans.*, 2002, 548.
26 P. J. Ellis, H. C. Freeman, M. A. Hitchman, D. Reinen and B. Wagner, *Inorg. Chem.*, 1994, **33**, 1249; V. M. Masters, M. J. Riley and M. A. Hitchman, *Inorg. Chem.*, 2001, **40**, 843.
27 D. L. Jameson and K. A. Goldsby, *J. Org. Chem.*, 1990, **55**, 4992.
28 G. M. Sheldrick, *Acta Crystallogr., Sect. A*, 1990, **46**, 467.
29 G. M. Sheldrick, SHELXL97, Program for the Refinement of Crystal Structures, University of Göttingen, Germany, 1997.
30 J. D. Dunitz, V. Schomaker and K. N. Trueblood, *J. Chem. Phys.*, 1988, **92**, 856.
31 L. J. Farrugia, *J. Appl. Crystallogr.*, 1999, **32**, 837.
32 F. E. Mabbs and D. Collison, *Electron Paramagnetic Resonance of d Transition Metal Compounds*; Elsevier; Amsterdam, The Netherlands, 1992, ch. 7.